Electronic Supplementary Information

for

A Disk-Type Polyarene Containing Four B←N Units

Yang Min, Chuandong Dou,* Hongkun Tian, Jun Liu* and Lixiang Wang

Y. Min, Dr. C. Dou, Prof. H. Tian, Prof. J. Liu, Prof. L. Wang
State Key Laboratory of Polymer Physics and Chemistry, Changchun Institute of Applied Chemistry, Chinese Academy of Sciences, Changchun 130022, P. R. China.
E-mail: chuandong.dou@ciac.ac.cn; liujun@ciac.ac.cn.
Y. Min
University of Chinese Academy of Sciences, Beijing 10039, P. R. China.

Contents

1. Experimental details

General. ^1H and ^{13}C NMR spectra were measured with a Bruker AV-400 (400 MHz for ^1H and 100 MHz for ^{13}C) spectrometer in $CDCl_3$ or C_6D_6 at 25 °C. ^{11}B NMR spectrum was measured with a Bruker AV III HD-500 spectrometer in $CDCl_3$ at 25 °C. Chemical shifts are reported in δ ppm using $CHCl_3$ (7.26 ppm) and C_6H_6 (7.16 ppm) for ^1H NMR, as well as using $CDCl_3$ (77.16 ppm) and C_6D_6 (128.06 ppm) for ^{13}C NMR as an internal standard. $BF_3 \cdot Et_2O$ was used for ^{11}B NMR as an external standard. Elemental analysis was performed on a VarioEL elemental analyzer. Thermal analysis was performed on a Perkin-Elmer 7 instrument under nitrogen flow at a heating rate of 10 °C min^{-1}. Differential scanning calorimetry (DSC) was measured with a Perkin-Elmer DSC 7 with a heating or cooling rate of 10 °C min^{-1}. UV/Vis absorption spectrum was measured with a Shimadzu UV-3600 spectrometer and fluorescence spectrum was measured with a Hitachi F-4500 spectrometer, respectively, in spectral grade solvents. Absolute fluorescence quantum yield was determined with a Edinburgh FLS920 calibrated integrating sphere system. Cyclic voltammetry (CV) was performed on an CHI660a electrochemical workstation using $n\mathrm{Bu}_4\mathrm{NClO}_4$ (0.1 M) as electrolyte at a scan rate of 50 mV s^{-1}. The CV cell consisted of a glassy carbon electrode, a Pt wire counter electrode, and a standard calomel reference electrode. The measurement was carried out under an argon atmosphene in CH_2Cl_2 (1.0 mM). The redox potentials were calibrated with ferrocene as an internal standard. The highest occupied molecular orbital (HOMO) and the lowest unoccupied molecular orbital (LUMO) energy levels were estimated by the equations: $E_{\mathrm{HOMO}}/E_{\mathrm{LUMO}} = -(4.80 + E_{1/2}^{\mathrm{ox}}/E_{1/2}^{\mathrm{red}})$ eV. Atomic force microscopy (AFM) was performed with a SPA300HV (Seiko Instruments, Inc., Japan) in tapping mode. The grazing incidence X-ray diffraction (GI-XRD) data was obtained on a Bruker D8 Discover reflector (Cu Kα, $\lambda = 1.54056$ Å) under 40 kV and 40 mA tube current. The scanning speed is 3 s per step with 0.1° step size (2θ). The in-plane X-ray diffraction (IP-XRD) data was obtained using a Rigaku SmartLab with an X-ray generation power of 40 kV tube voltage and 30 mA tube current. The diffraction was recorded in the $2\theta-\chi$ mode. The scanning speed is 5 s per step with 0.02° step size (2θ).

Materials and reagents. All reactions were performed under an argon atmosphere, unless stated otherwise. Commercially available solvents and reagents were used without further purification unless otherwise mentioned. Dry toluene and CH_2Cl_2 were distilled via standard methods. Quinoxalino[2,3-b]phenazine-6,13-dione (**2**) was prepared according to the literature methods.[1]

2. Syntheses and characterizations

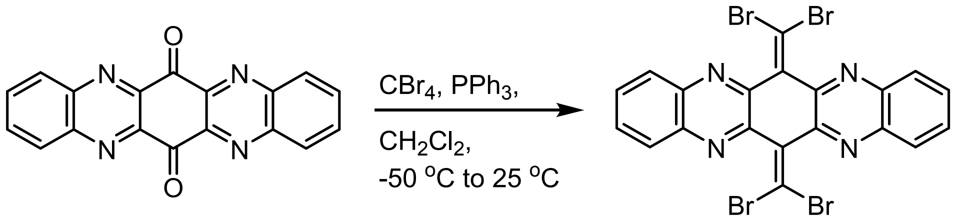

2 **3** (78%)

6,13-bis(dibromomethylene)-6,13-dihydroquinoxalino[2,3-b]phenazine (3): Under argon, triphenylphosphine (1.32 g, 3.97 mmol) and tetrabromomethane (2.0 g, 7.68 mmol) were placed in a three-necked flask, followed by adding dry CH_2Cl_2 (50 mL) at −15 °C. After the mixture was stirred at −15 °C for 1 h, quinoxalino[2,3-b]phenazine-6,13-dione **2** (0.20 g, 0.64 mmol) was added slowly under argon. Then the mixture was stirred for 8 h at 25 °C. After removing the solvents in reduced pressure, the mixture was purified by silica gel column chromatography (CH_2Cl_2:Et_2O = 10:1). **3** was obtained as a yellow crystalline solid in 78% yield (0.31 g). ^1H NMR (400 MHz, $CDCl_3$, 25 °C): δ (ppm) 8.16 (m, 1H, CH), 7.84 (s, 1H, CH). ^{13}C NMR(100 MHz, $CDCl_3$, 25 °C): δ (ppm) 146.69, 140.59, 134.99, 131.34, 129.51, 101.87. Anal. Calcd for $C_{20}H_8Br_4N_4$: C, 38.50; H, 1.29; N, 8.98. Found: C, 38.65; H, 1.36; N, 8.79.

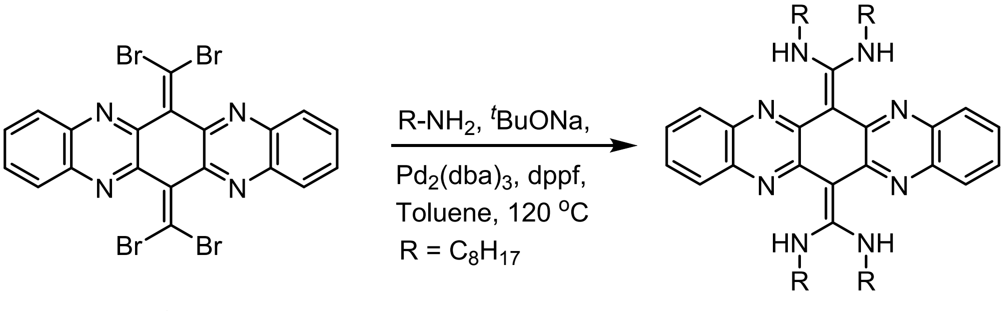

3 **4** (55%)

1,1'-(quinoxalino[2,3-b]phenazine-6,13-diylidene)bis(N,N'-dioctylmethanediamine) (4): **3** (200.0 mg, 0.32 mmol), $Pd_2(dba)_3$ (8.8 mg, 0.0096 mmol), 1,1'-bis(diphenylphosphino)ferrocene (dppf) (21.4 mg, 0.039 mmol) and sodium *tert*-butoxide (246.5 mg, 2.57 mmol) were placed in a three-necked flask under argon. Then dried toluene (40 mL) and octylamine (331.4 mg, 2.56 mmol) were added. The mixture was stirred at 120 °C for 20 h. After cooling down, the mixture was extracted using water and CH_2Cl_2. The combined organic phase was dried over anhydrous Na_2SO_4, filtered and concentrated under reduced pressure. The crude product was first purified by column chromatography on silica gel with CH_2Cl_2:hexane:Et_3N = 2:1:0.03 as the eluent. After further purified by silica gel column chromatography (CH_2Cl_2:EtOAc = 1:1), **4** was obtained as a dark red solid in 56% yield (146 mg). ^{1}H NMR (400 MHz, C_6D_6, 25 °C): δ (ppm) 14.47 (s, 4H, NH), 7.50 (m, 4H, CH), 7.19 (m, 4H, 4H), 3.25 (m, 8H, CH_2), 1.67 (m, 8H, CH_2), 1.39−1.24 (m, 40H, CH_2), 0.90 (t, J = 8.0 Hz, 12H, CH_3). ^{13}C NMR(100 MHz, C_6D_6, 25 °C): δ (ppm) 166.00, 151.10, 137.46, 124.96, 124.04, 90.36, 46.93, 32.16, 30.59, 29.71, 29.63, 27.64, 23.01, 14.31. Anal. Calcd for $C_{52}H_{80}N_8$: C, 76.42; H, 9.87; N, 13.71. Found: C, 76.58; H, 9.76; N, 13.71.

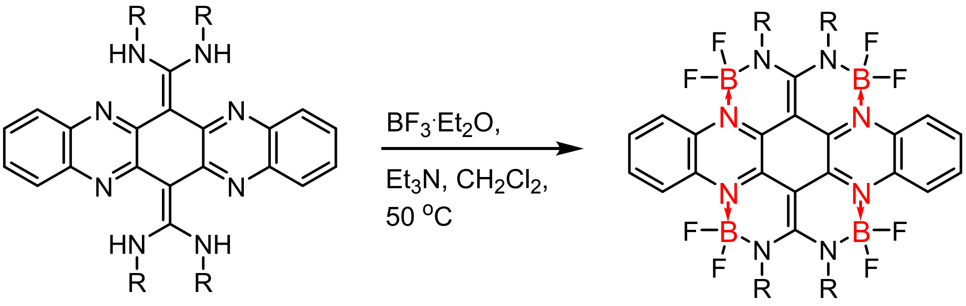

4 R = C_8H_{17} **1a** (76%)

2,2,7,7,10,10,15,15-octafluoro-1,8,9,16-tetraoctyl-1,2,7,8,9,10,15,16-octahydro-1,2aλ^4,6bλ^4,8,9,10aλ^4,14bλ^4,16-octaaza-2λ^4,7λ^4,10λ^4,15λ^4-tetraboradibenzo[*d,m*]coronene (1a): Under argon, $BF_3·Et_2O$ solution (1.62 mL, 5.84 mmol) was added to a solution of **3** (59.0 mg, 0.073 mmol) and Et_3N (0.41 mL) in dry CH_2Cl_2 (12 mL). The mixture was stirred at 50 °C for 4 h. After removing the solvents in reduced pressure, the blue mixture was purified by silica gel column chromatography (CH_2Cl_2). The obtained solid was then extracted using water and hexane. The combined organic phase was dried over anhydrous Na_2SO_4, filtered and concentrated under reduced pressure to give **1a** in 76% yield (56.0 mg). ^{1}H NMR (400 MHz, $CDCl_3$, 25 °C): δ (ppm) 8.72 (q, 4H, CH), 6.91 (q, 4H, CH), 3.88 (t, J = 8.0 Hz, 8H, CH_2), 1.90 (m, 8H, CH_2), 1.36−1.22 (m, 40H, CH_2), 0.87 (t, J = 8.0 Hz, 12H). ^{13}C NMR(100 MHz, $CDCl_3$, 25 °C): δ (ppm) 156.17, 139.38, 131.12, 128.96, 123.25, 123.17, 123.09, 98.19, 46.62, 32.12, 29.64, 29.56, 28.59, 27.25, 23.03, 14.31. Anal. Calcd for $C_{52}H_{76}B_4F_8N_8$: C, 61.93; H, 7.60; N, 11.11. Found: C, 61.82; H, 7.69; N, 11.21.

3. X-ray crystallographic analysis

Single crystal X-ray diffraction measurements were performed by Rigaku SmartLab X-ray diffractometer with Cu Kα radiation (λ = 1.5418 Å). The structures were solved by direct method (SHELXL-97) and refined by the full-matrix least-squares on F^2 (SHELXL-97). CCDC 1887849 (**3**) contains the supplementary crystallographic data for this paper. The data can be obtained free of charge from The Cambridge Crystallographic Data Centre via www.ccdc.cam.ac.uk/data_request/cif.

Single crystals of **3** suitable for X-ray crystallographic analysis were obtained by recrystallization from $CHCl_3/CH_3OH$ solutions. Crystal data of **3**: $C_{20}H_8Br_4N_4$; FW = 623.94, monoclinic, space group P 21/n, $a = 7.3870(9)$ Å, $b = 15.2414(18)$ Å, $c = 17.567(2)$ Å, $\alpha = 90°$, $\beta = 98.727(2)°$, $\gamma = 90°$, $V = 1954.9(4)$ Å^3, $Z = 4$, $D_{\mathrm{calcd}} = 2.120$ g cm^{-3}, $\mu = 8.249$ mm^{-1}, $R_1 = 0.0335$ ($I > 2\sigma(I)$), w$R_2 = 0.1156$ (all data), GOF = 1.020. Total 10995 reflections were collected, among which 3979 reflections were independent ($R_{\mathrm{int}} = 0.0266$).

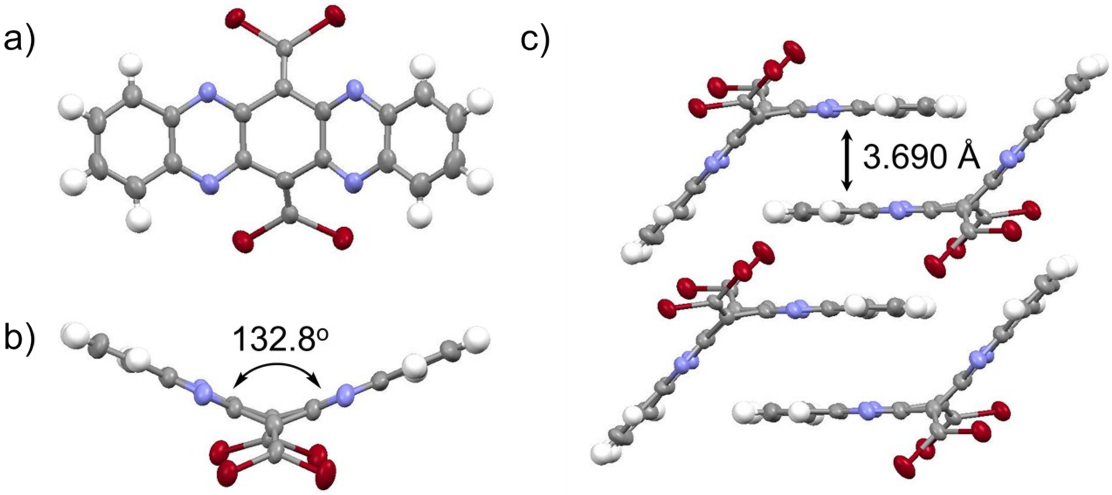

Fig. S1. a) Crystal structure of **3**, which exhibits the saddle-like conformation with the bent angle of 132.8°; c) Packing structure of **3** with the π–π stacking distance of 3.690 Å.

4. Structural analysis

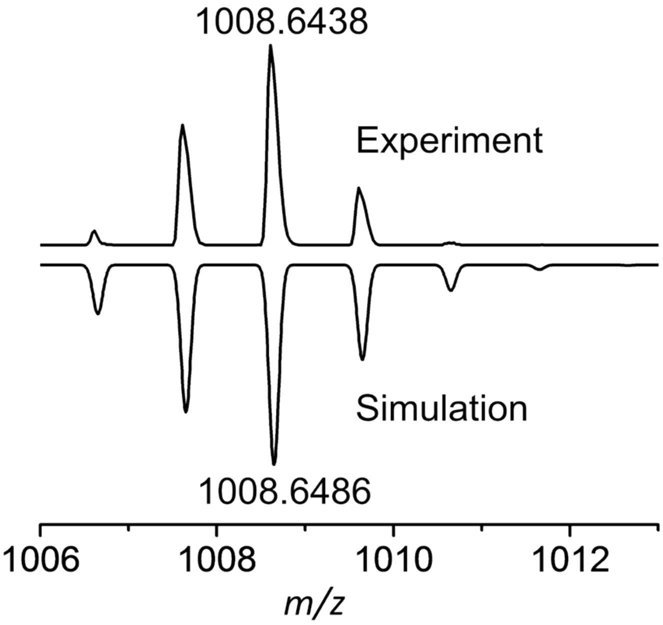

Fig. S2. High-resolution MALDI-TOF MS spectrum of **1a** with the corresponding experimental and simulated isotopic distributions.

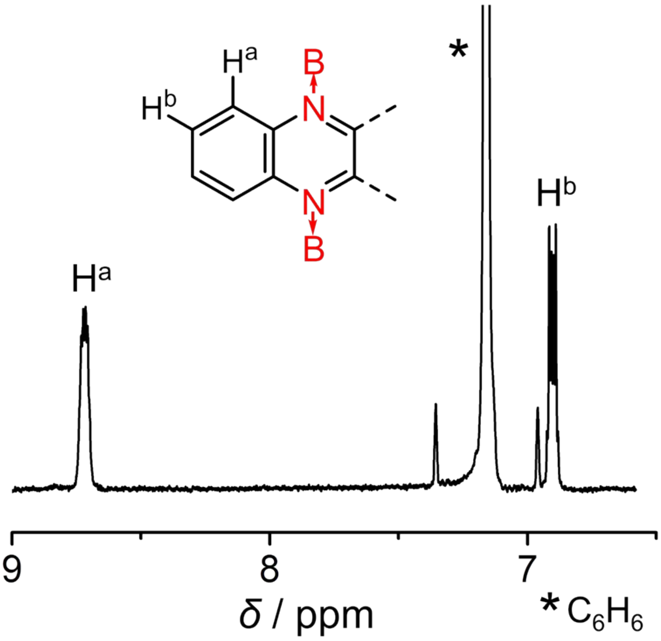

Fig. S3. Aromatic region of ^{1}H NMR spectrum of **1a** in C_6D_6.

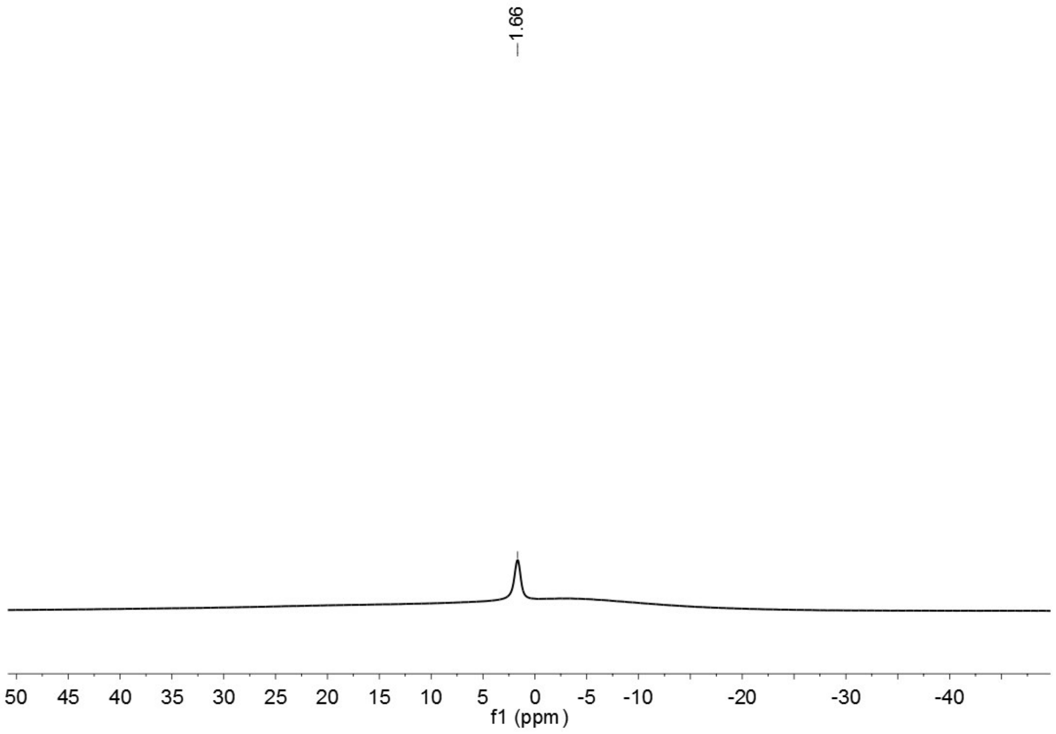

Fig. S4. ^{11}B NMR spectrum of **1a** in $CDCl_3$.

5. Thermal properties

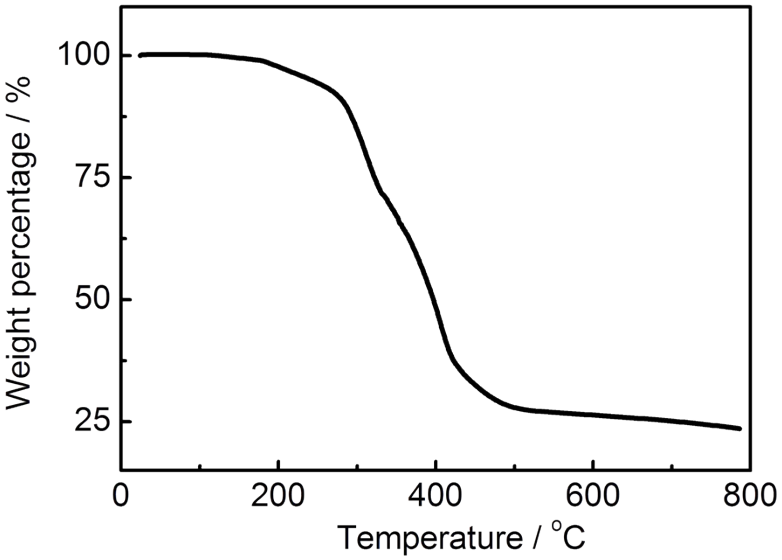

Fig. S5. Thermogravimetric analysis (TGA) of **1a**. **1a** has good thermal stability with thermal decomposition temperature (T_d) at 5% weight loss of 242 °C.

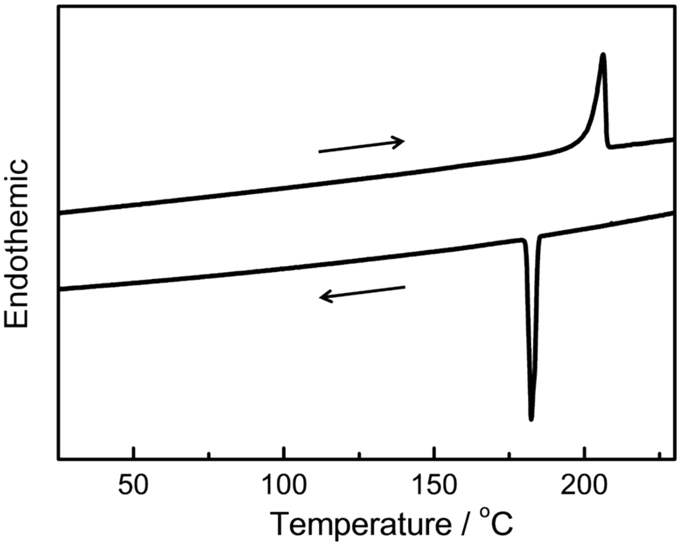

Fig. S6. Differential scanning calorimetry (DSC) analysis (the first cooling and the second heating curves) of **1a**, indicating its melting point at 206 °C.

6. Geometry optimizations, NICS, DFT and TD-DFT calculations

1b is the model compounds for **1a** with methyl chain on the sp^3 N atom in place of octyl chain. **5** is the corresponding polycyclic aromatic hydrocarbons with C−C unit, which is the analogue of **1a**. The geometry optimizations of **1b** and **5** were performed using Gaussian 09 program at the B3LYP/6-31G(d,p) level of theory.[2] Density functional theory (DFT) calculations at the B3LYP/6-31G(d,p) level of theory were performed on **1b** and **5**. Nucleus-independent chemical shift (NICS) calculations were performed at the B3LYP/6-311+G(d,p) level of theory using the geometries optimized at the B3LYP/6-31G(d,p) level. To assign the absorption bands observed in the UV/Vis spectrum, time-dependent DFT calculation was performed on **1b** using Gaussian 09 program at the B3LYP/6-31G(d,p) level of theory.

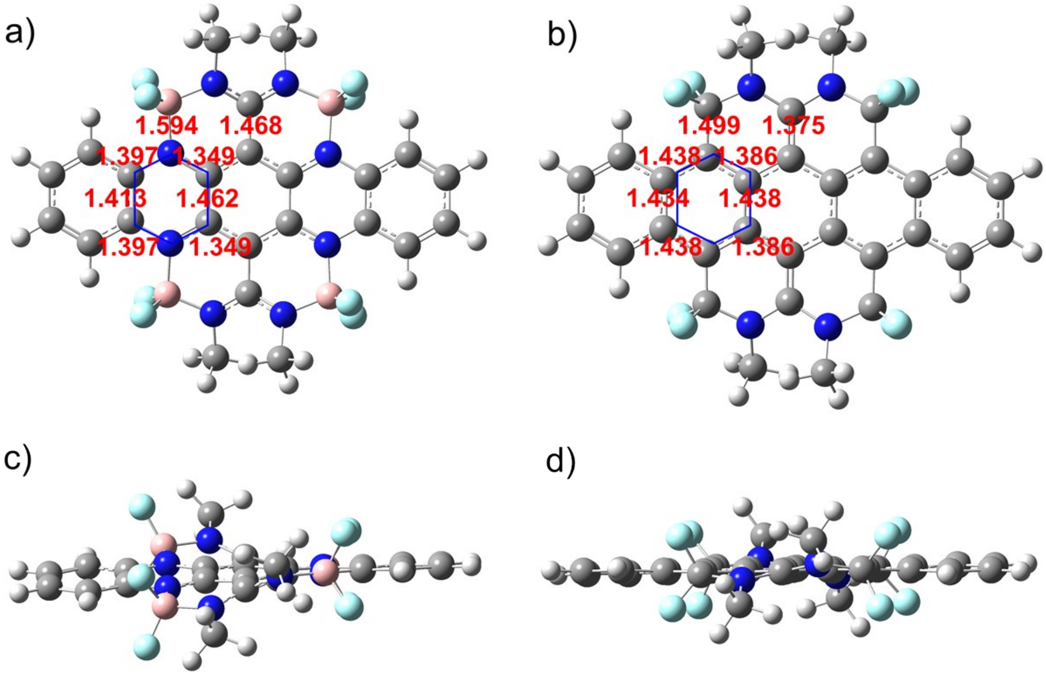

Fig. S7. The optimized structures of a,c) **1b** and b,d) **5** calculated at the B3LYP/6-31G(d,p) level of theory, together with some bond lengths.

Table S1. Coordinates of the optimized structure for **1b** at the B3LYP/6-31G(d,p) level.

Atom	x	y	z
C	1.23328200	0.72922600	-0.05181900
C	0.00009100	1.42982400	-0.00009400
C	0.00019800	2.89790900	0.00065400
C	3.62652300	0.70116600	-0.08418800
C	1.23317900	-0.72936200	0.05135600
C	3.62643800	-0.70167500	0.08296300
C	-0.00018800	-2.89793500	0.00015000
C	-0.00009700	-1.42981300	-0.00005900
C	-1.23328200	-0.72920600	-0.05182500
C	-1.23321200	0.72937900	0.05120100
C	6.04756700	-0.69662600	0.08352000
C	6.04765500	0.69562800	-0.08609400
C	-3.62651500	-0.70122600	-0.08391600
C	-3.62646400	0.70170800	0.08248600
C	-4.85677800	1.39001800	0.16678500
H	-4.86686900	2.46116200	0.28069400
C	-4.85684500	-1.38942800	-0.16871700
H	-4.86701600	-2.46054700	-0.28289800
C	-6.04763400	-0.69586700	-0.08528000
H	-6.98446100	-1.23969500	-0.14895000
C	-6.04760000	0.69655600	0.08298600
H	-6.98440400	1.24046500	0.14630400
B	-2.49107600	-2.94929300	-0.42995600
F	-3.11233100	-3.12829700	-1.65810500
F	-3.20901000	-3.56190900	0.59235400
C	-1.00295900	-4.88260000	-1.03497300
H	-0.00574400	-5.06417800	-1.43668300
H	-1.26073100	-5.66746100	-0.31926900
H	-1.72452300	-4.91131200	-1.85120800
H	6.98434400	-1.24052100	0.14734500
H	6.98450400	1.23933600	-0.15047500
C	4.85670800	-1.38995800	0.16793600
H	4.86676100	-2.46100200	0.28281400
C	4.85688800	1.38919500	-0.16987900
H	4.86711300	2.46021500	-0.28494300
N	1.07863400	-3.53105500	0.46090800
N	-1.07909700	-3.53104800	-0.46058000
B	2.49066700	-2.94929100	0.43107200
F	3.20915600	-3.56318400	-0.59010900
F	3.11103500	-3.12709800	1.65980200
C	1.00258100	-4.88274300	1.03498200

H	0.00539400	-5.06445900	1.43669900
H	1.26038600	-5.66739700	0.31907500
H	1.72415800	-4.91159700	1.85120900
N	1.07916300	3.53131700	-0.45939600
N	-1.07864700	3.53089100	0.46172900
C	1.00314600	4.88349000	-1.03233100
H	0.00596000	5.06558100	-1.43387500
H	1.26096500	5.66750600	-0.31572200
H	1.72472400	4.91305500	-1.84853500
C	-1.00220800	4.88196400	1.03720100
H	-0.00495100	5.06295700	1.43909400
H	-1.25971700	5.66747100	0.32211700
H	-1.72379800	4.91023300	1.85343600
N	2.40901000	1.38318000	-0.14690100
N	2.40883700	-1.38346500	0.14639400
N	-2.40899800	-1.38318400	-0.14676600
B	2.49104000	2.94923200	-0.43053400
B	-2.49073400	2.94947300	0.43045300
F	3.11095400	3.12772600	-1.65943000
F	3.21015300	3.56215400	0.59075200
F	-3.11224400	3.12744600	1.65857400
F	-3.20822800	3.56325400	-0.59149100
N	-2.40887000	1.38350800	0.14592900

Table S2. Coordinates of the optimized structure for **5** at the B3LYP/6-31G(d,p) level.

Atom	x	y	z
C	-1.26579800	-0.71848900	-0.01962800
C	-0.00014700	-1.41365900	0.00013200
C	-0.00038000	-2.78858300	0.00135000
C	-3.72989700	-0.71645300	0.01758700
C	-1.26558900	0.71880500	0.01950000
C	-3.72965300	0.71751500	-0.01935100
C	0.00047800	2.78855400	0.00074900
C	0.00029500	1.41362300	0.00039200
C	1.26597800	0.71845500	-0.01928100
C	1.26577700	-0.71882600	0.01922100
C	-6.16913500	0.70319000	-0.04867900
C	-6.16940800	-0.70135100	0.04388400
C	3.73004300	0.71642700	0.01836500
C	3.72980200	-0.71752300	-0.01997900
C	4.97833600	-1.39473300	-0.07731600
H	4.99591900	-2.47247400	-0.14695300
C	4.97886500	1.39323500	0.07416200
H	4.99689700	2.47098000	0.14361200

C	6.16955500	0.70125800	0.04509600
H	7.10875300	1.24452700	0.08966000
C	6.16928300	-0.70314400	-0.04968800
H	7.10825400	-1.24670200	-0.09547400
F	3.27218100	3.36376300	-1.05794100
F	3.02109300	3.45150600	1.10052600
C	1.13061900	4.79897400	-0.94571100
H	0.10981400	5.00331700	-1.25854500
H	1.49220000	5.61497500	-0.31341500
H	1.75839500	4.73638200	-1.83300300
H	-7.10810700	1.24682800	-0.09349600
H	-7.10860400	-1.24470200	0.08745400
C	-4.97818700	1.39481500	-0.07548800
H	-4.99579500	2.47265500	-0.14353200
C	-4.97871300	-1.39335700	0.07214800
H	-4.99675800	-2.47120300	0.13998900
N	-1.15952800	3.50499100	0.24255800
N	1.16066600	3.50484600	-0.24069100
F	-3.02023800	3.45344700	-1.09821600
F	-3.27098700	3.36353900	1.06019500
C	-1.12919600	4.79920200	0.94738700
H	-0.10842600	5.00312200	1.26063300
H	-1.49015100	5.61528700	0.31483900
H	-1.75740200	4.73697300	1.83439300
N	-1.16050600	-3.50508300	-0.23949100
N	1.15971900	-3.50481800	0.24369100
C	-1.13032100	-4.80200300	-0.93928000
H	-0.10953200	-5.00741300	-1.25149300
H	-1.49171700	-5.61547900	-0.30363400
H	-1.75836000	-4.74295500	-1.82661300
C	1.12966100	-4.79583000	0.95445600
H	0.10856000	-4.99954000	1.26670300
H	1.49265700	-5.61436700	0.32626800
H	1.75608600	-4.72900700	1.84243000
F	-3.27007900	-3.36246700	-1.06225600
F	-3.02426300	-3.45243400	1.09669300
F	3.27322300	-3.36521400	1.05534900
F	3.01680800	-3.45222700	-1.10255000
C	2.44436800	2.90559300	-0.04832100
C	2.46873900	1.40731600	-0.00438600
C	2.46832900	-1.40803000	0.00399800
C	2.44333300	-2.90636000	0.04791000
C	-2.44339700	2.90622100	0.04995900
C	-2.46813300	1.40800900	0.00464700
C	-2.46855600	-1.40733800	-0.00511700
C	-2.44441700	-2.90550700	-0.05013300

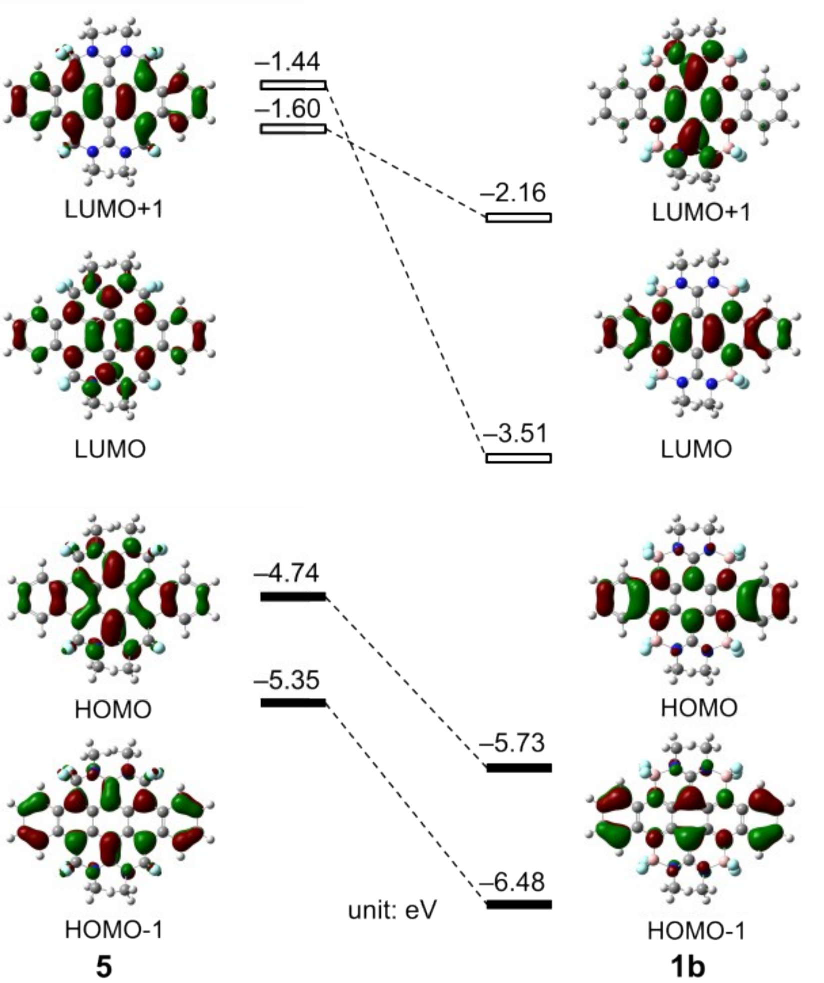

Fig. S8. Kohn-Sham molecular orbitals of **5** and **1b**, calculated at the B3LYP/6-31G(d,p) level of theory.

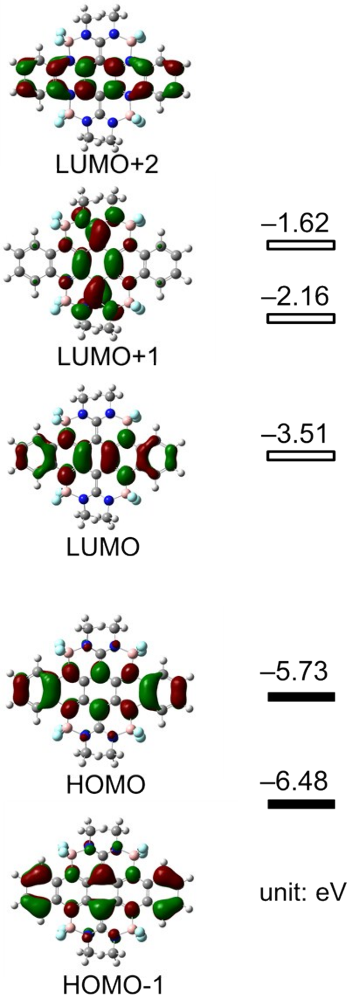

Excited state 1
Energy: 2.28 eV
Wavelength: 544 nm
Oscillator strength: 0.6203
Configurations: HOMO-1→LUMO+2 (0.13250)
HOMO→LUMO (0.70370)
HOMO←LUMO (−0.13066)

Excited state 2
Energy: 2.42 eV
Wavelength: 512 nm
Oscillator strength: 0.0002
Configurations: HOMO-1→LUMO (0.70305)

Fig. S9. The molecular orbitals, energy levels, excitation energies and oscillator strengths of **1b**, based on the TD-DFT (B3LYP/6-31G(d,p)) calculation. The main absorption band of **1a** is assignable to electronic HOMO→LUMO and HOMO−1→LUMO+2 transitions. These transitions are all dominated by the fused-quinoxaline moieties, suggesting that the π-framework is responsible for the intensive absorption of **1a**.

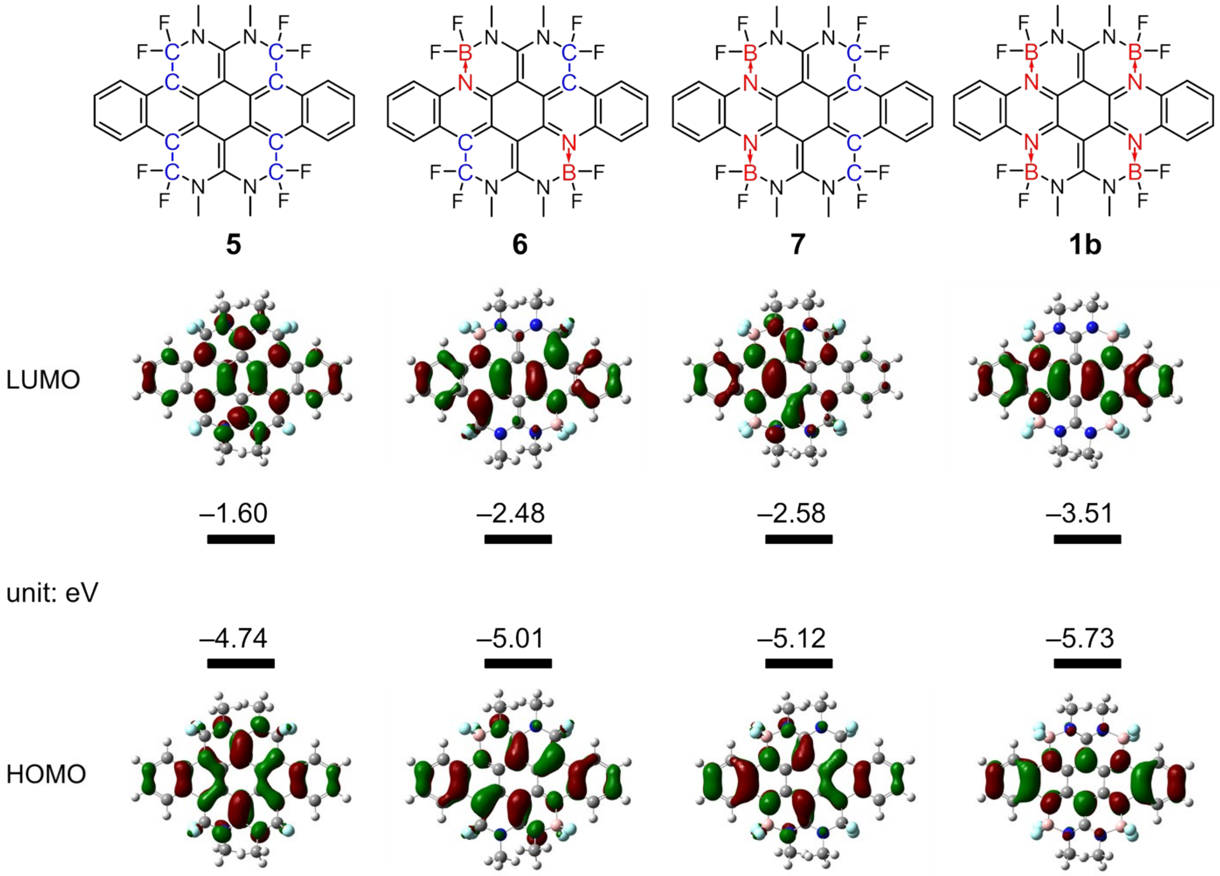

Fig. S10. Chemical structures and Kohn-Sham molecular orbitals of **5**, **6**, **7** and **1b**, calculated at the B3LYP/6-31G(d,p) level of theory.

We also performed DFT calculations on the analogs containing two B←N units and two C−C units **6** and **7**, which only have the B←N units on different positions. The molecular orbitals and energy levels of **5**, **6**, **7** and **1b** are fully compared in Fig. S10. They display the different distributions of LUMOs and HOMOs, and the different LUMO/HOMO energy levels. From **5** to **6**/**7**, the LUMO and HOMO energy levels are decreased by ca. 0.9 eV and 0.3 eV, respectively. From **6**/**7** to **1b**, the LUMO and HOMO energy levels are decreased by ca. 1.0 eV and 0.7 eV, respectively. It is suggested that more B←N units can further decrease the energy levels and enhance the electron affinities of π-systems, which is very desirable for the development of n-type organic semiconductors.

7. Photophysical properties

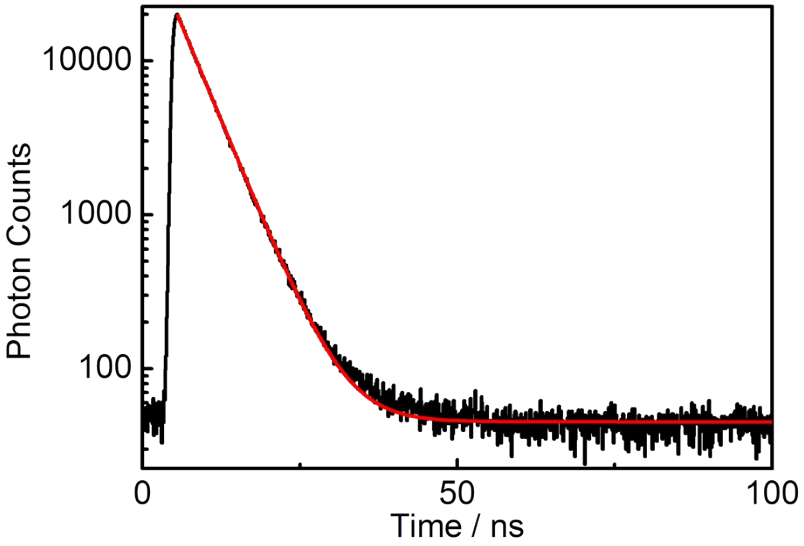

Fig. S11. Fluorescence decay profile (black line) of **1a** in toluene. The red line is the theoretical fit. The excited wavelength is 375 nm, and the fluorescence wavelength is 631 nm. The fluorescence lifetime is measured as 4.4 ns.

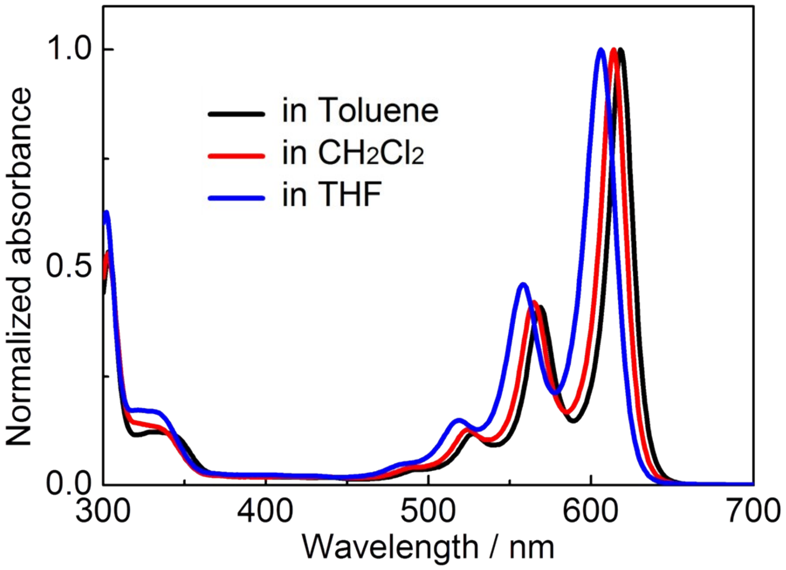

Fig. S12. UV/Vis absorption spectra of **1a** in various solutions. The absorption peaks are 618/569 nm for the toluene solution, 614/565 nm for the CH_2Cl_2 solution and 606/558 nm for the THF solution, respectively.

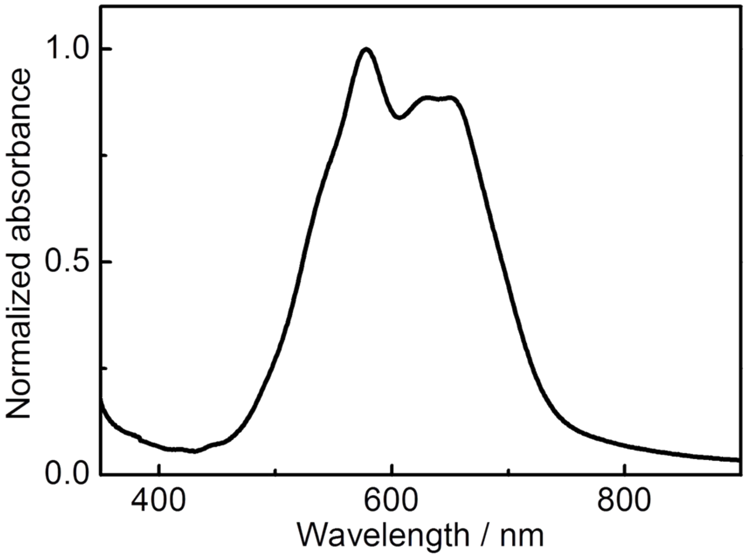

Fig. S13. UV/Vis absorption spectrum of **1a** in thin film. The absorption peaks are 650/630/578 nm, which are red-shifted and broadened in comparison to that of **1a** in toluene solution.

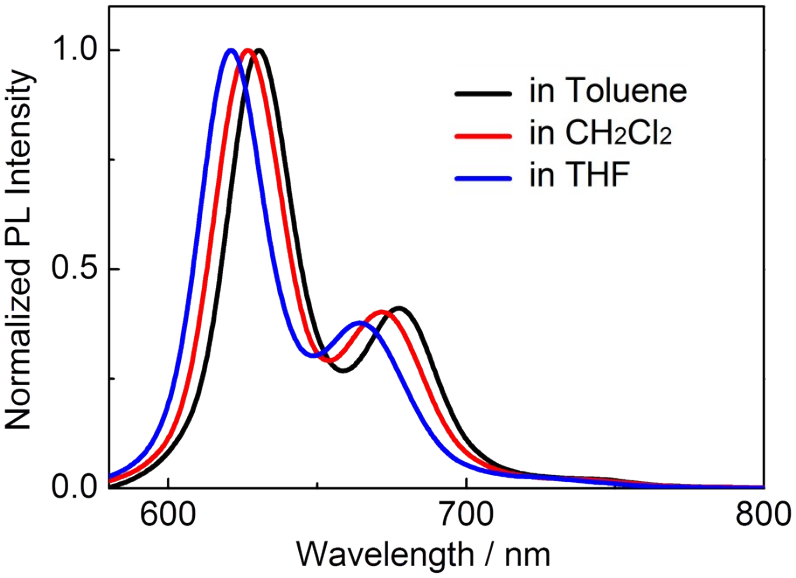

Fig. S14. Fluorescence spectra of **1a** in various solutions. The fluorescence peaks are 631/670 nm for the toluene solution, 627/672 nm for the CH_2Cl_2 solution and 621/664 nm for the THF solution, respectively.

8. OFET fabrications and characterizations

Solution-processed organic field-effect transistors (OFETs) were fabricated with a bottom-gate/top-contact (BGTC) configuration. The substrates with silicon wafer covered with 300 nm SiO_2 were first cleaned with double-distilled water, acetone and isopropanol in an ultrasonic bath and then dried under a nitrogen flow. The substrates were then modified with n-octyltrichlorosilane (OTS) self-assembled monolayer (SAM) according to literature procedures. The solution of **1a** in $CHCl_3$ (10 mg/mL) was spin-casted, followed by thermal annealing at 160 ^{o}C for 10 min. Finally, Au source and drain electrodes (~40 nm) with W/L = 5 (W = 1.0 mm, L = 0.2 mm) were deposited. Field-effect mobility was calculated in the saturation regime by using the equation: $I_{DS}^{sat} = (\mu C_i W/2L)(V_{GS}-V_T)^2$, where I_{DS} is the drain-source current, μ is the field-effect mobility, C_i is the capacitance per unit area of the gate dielectric layer, V_{GS} and V_T are the gate voltage and threshold voltage, respectively.

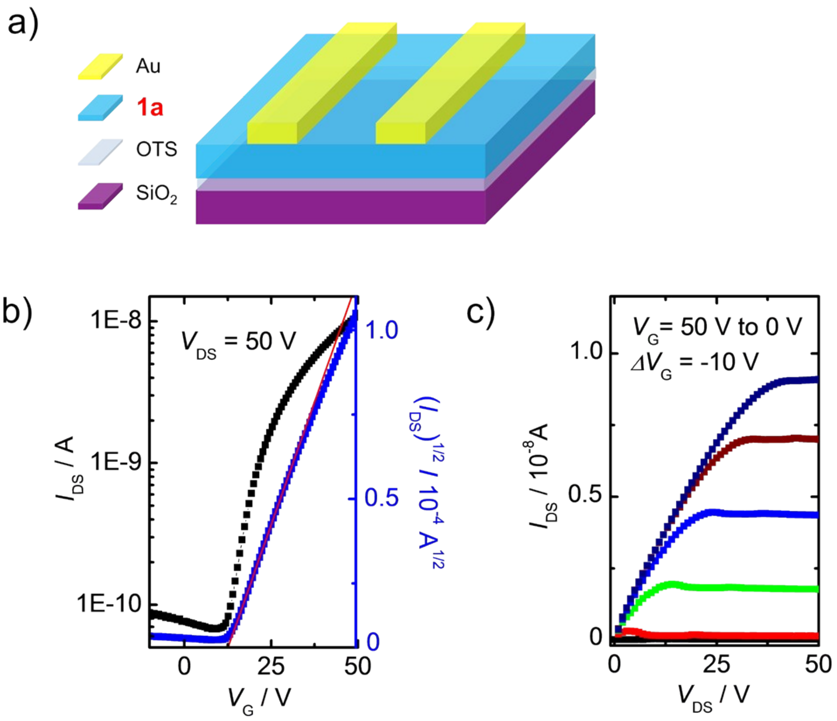

Fig. S15. a) Schematic drawing of the OFET device configuration; c) Transfer and d) output curves of the OFET device. We have fabricated six devices at this optimized condition and each device was tested over 4 times. The device shows the unipolar n-type characteristic with an average electron mobility (μ_e) of 3.40 × 10^{-4} cm^2 V^{-1} s^{-1}, an on/off current ratio (I_{on}/I_{off}) value of 10^2–10^3, and a threshold voltage (V_T) of 10 V.

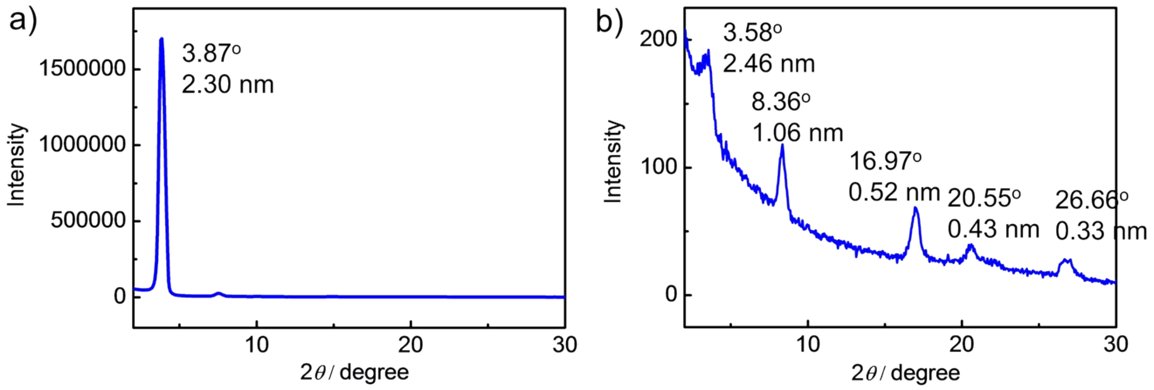

Fig. S16. a) The grazing incidence X-ray diffraction (GI-XRD) curve and b) the in-plane X-ray diffraction (IP-XRD) curve of the active layer of the device. The complicated diffraction peaks probably indicate the polycrystalline nature of the prepared film.

9. ^{1}H NMR and ^{13}C NMR spectra

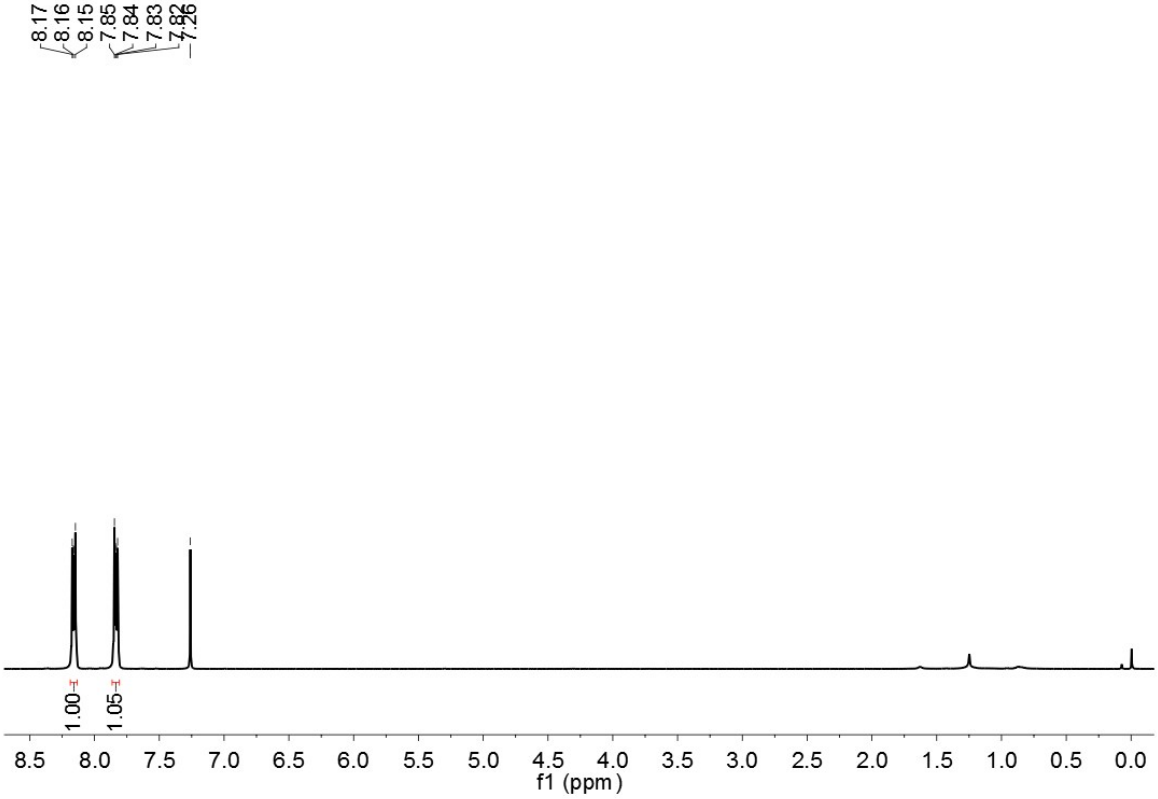

Fig. S17. ^{1}H NMR spectrum of **3** in $CDCl_3$.

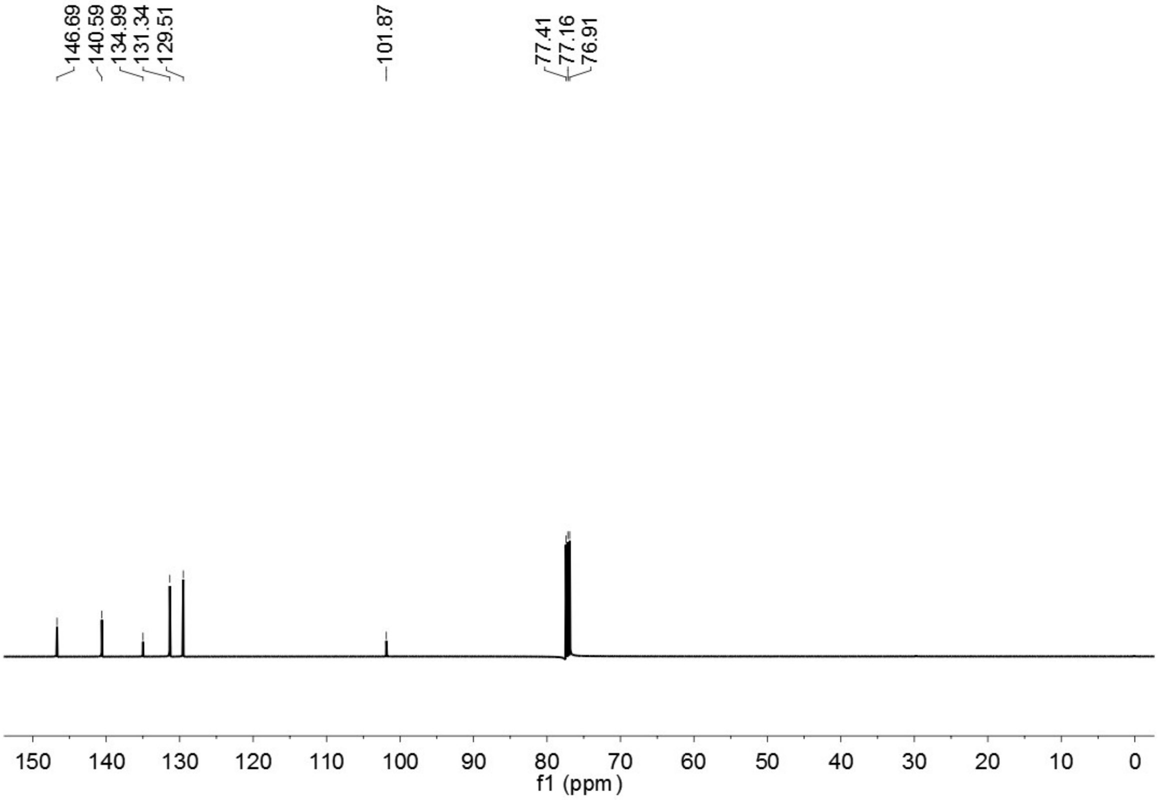

Fig. S18. ^{13}C NMR spectrum of **3** in $CDCl_3$.

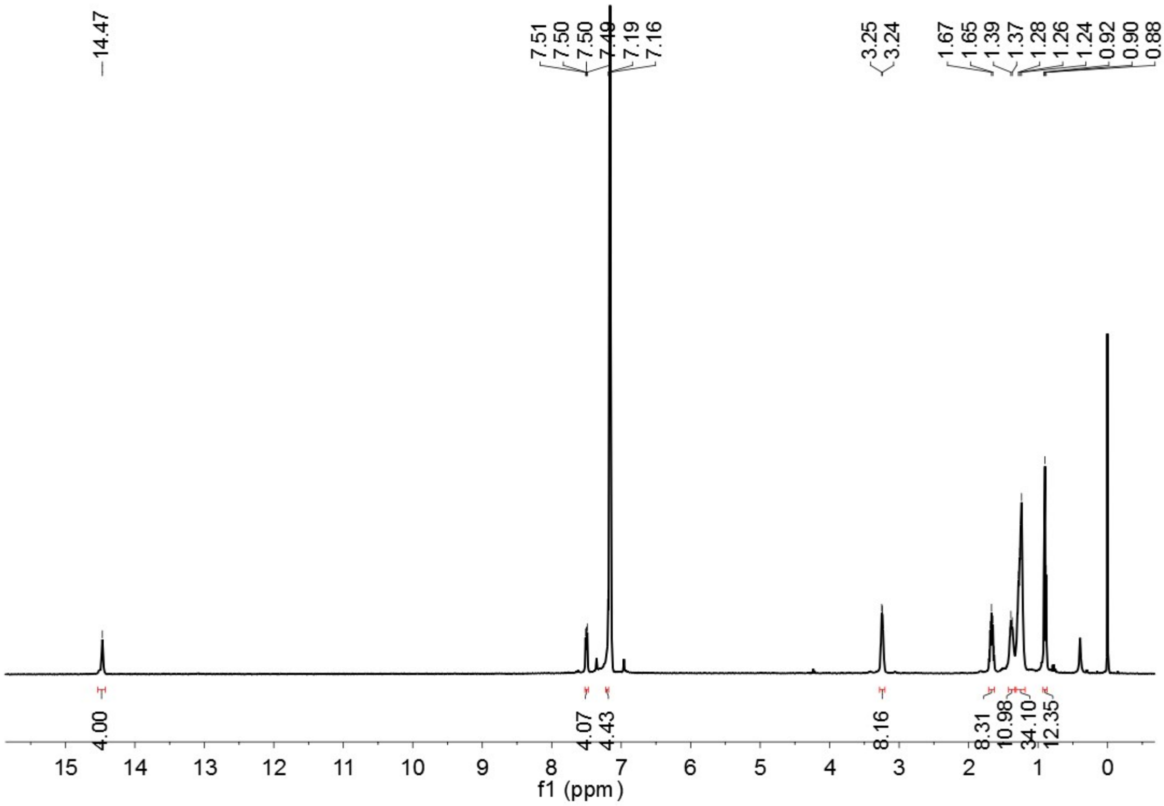

Fig. S19. ^{1}H NMR spectrum of **4** in C_6D_6.

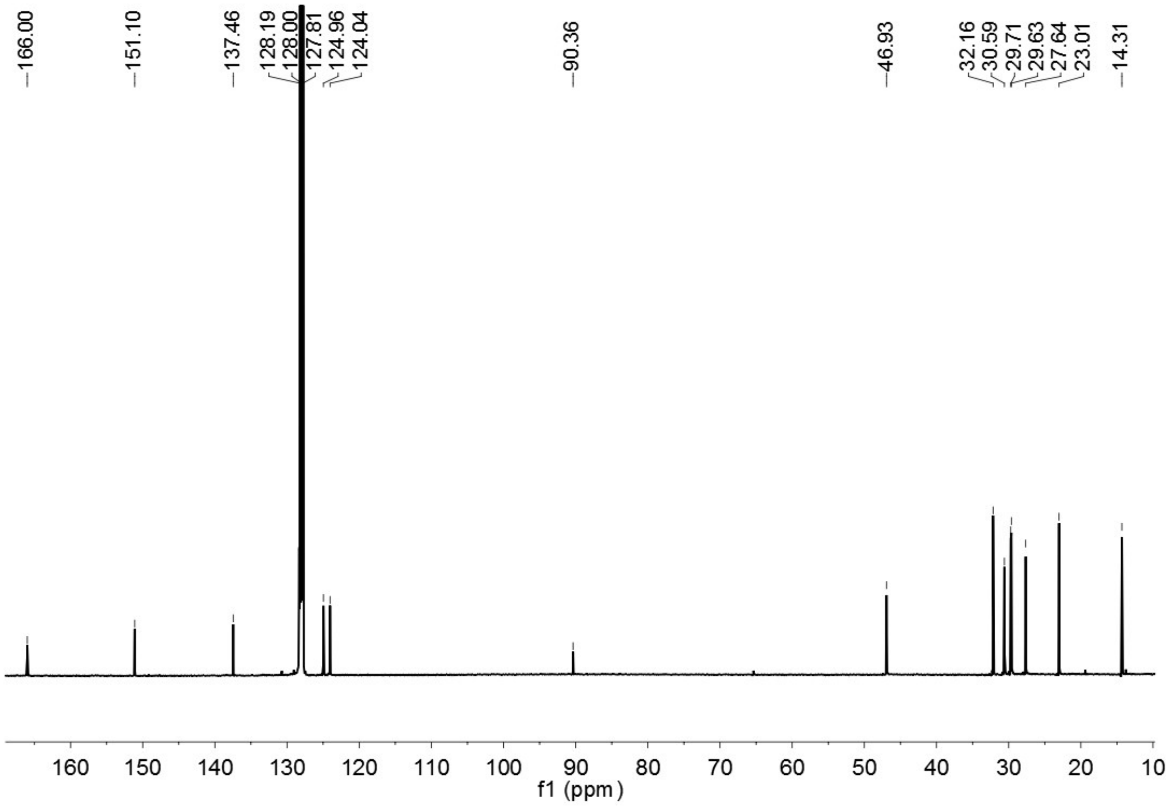

Fig. S20. ^{13}C NMR spectrum of **4** in C_6D_6.

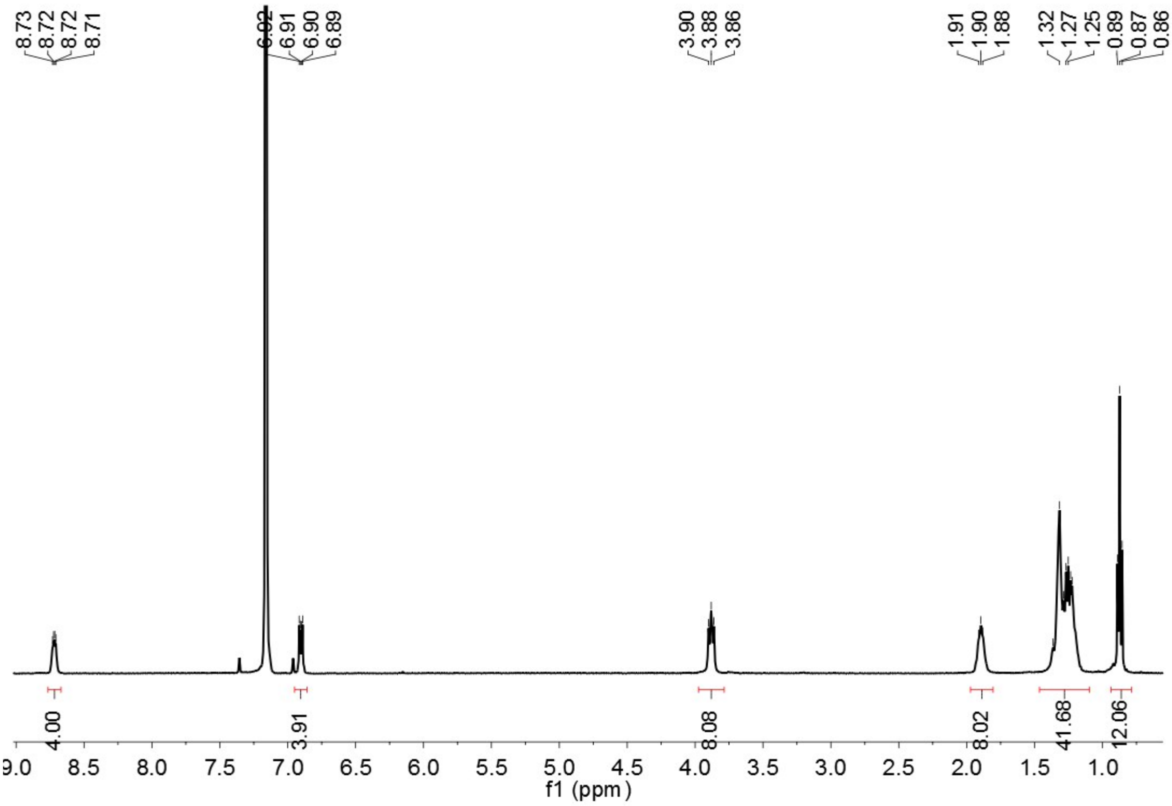

Fig. S21. ^{1}H NMR spectrum of **1a** in CDCl$_3$.

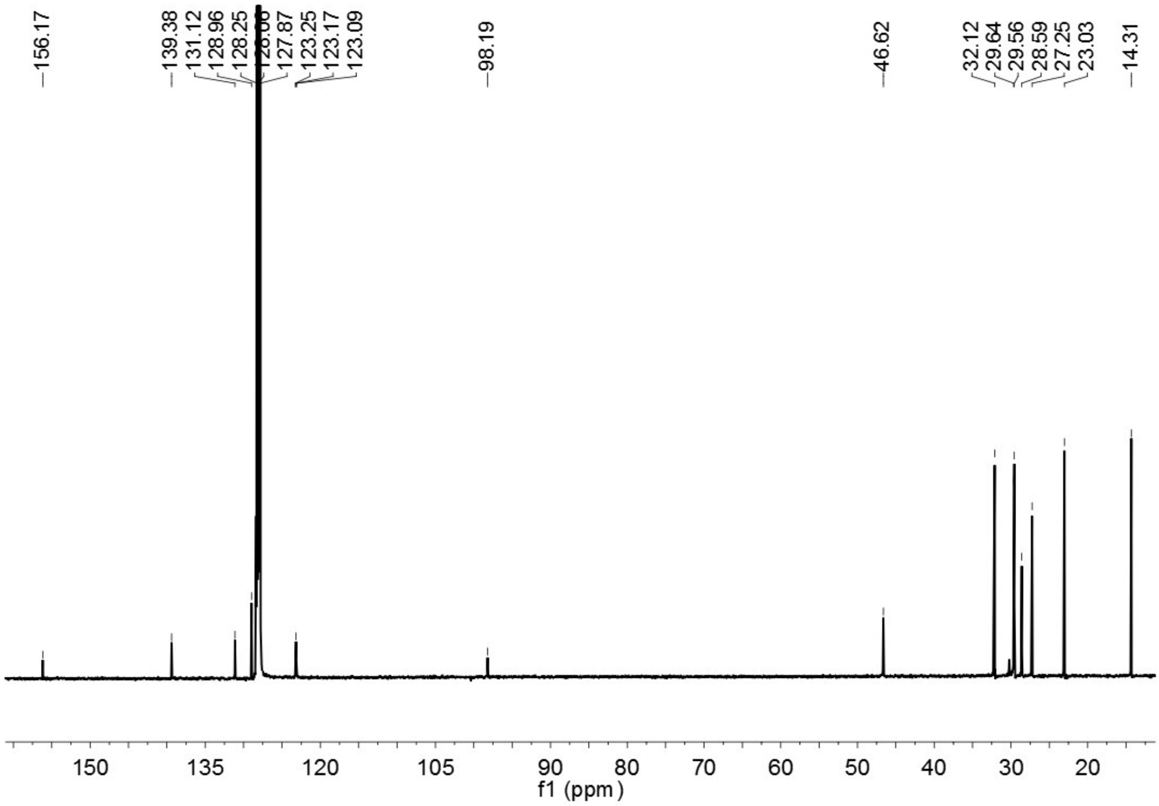

Fig. S22. ^{13}C NMR spectrum of **1a** in CDCl$_3$.

10. Reference

1 (a) G. M. Badger and R. Pettit, *J. Chem. Soc.,* 1951, 3211; (b) S. Miao, A. L. Appleton, N. Berger, S. Barlow, S. R. Marder, K. I. Hardcastle and U. H. F. Bunz, *Chem. Eur. J.,* 2009, **15**, 4990.

2 Gaussian 09 (Revision A.02), M. J. Frisch, G. W. Trucks, H. B. Schlegel, G. E. Scuseria, M. A. Robb, J. R. Cheeseman, G. Scalmani, V. Barone, B. Mennucci, G. A. Petersson, H. Nakatsuji, M. Caricato, X. Li, H. P. Hratchian, A. F. Izmaylov, J. Bloino, G. Zheng, J. L. Sonnenberg, M. Hada, M. Ehara, K. Toyota, R. Fukuda, J. Hasegawa, M. Ishida, T. Nakajima, Y. Honda, O. Kitao, H. Nakai, T. Vreven, J. A. Montgomery, Jr., J. E. Peralta, F. Ogliaro, M. Bearpark, J. J. Heyd, E. Brothers, K. N. Kudin, V. N. Staroverov, R. Kobayashi, J. Normand, K. Raghavachari, A. Rendell, J. C. Burant, S. S. Iyengar, J. Tomasi, M. Cossi, N. Rega, J. M. Millam, M. Klene, J. E. Knox, J. B. Cross, V. Bakken, C. Adamo, J. Jaramillo, R. Gomperts, R. E. Stratmann, O. Yazyev, A. J. Austin, R. Cammi, C. Pomelli, J. W. Ochterski, R. L. Martin, K. Morokuma, V. G. Zakrzewski, G. A. Voth, P. Salvador, J. J. Dannenberg, S. Dapprich, A. D. Daniels, Ö. Farkas, J. B. Foresman, J. V. Ortiz, J. Cioslowski and D. J. Fox, *Gaussian, Inc*., Wallingford CT, 2009.